「Investigation of radiosensitizing effects of 4-methylumbelliferone in radioresistant cancer cells」

(4-メチルウンベリフェロンによる放射線抵抗性癌細胞の放射線増感効果の検討)

弘前大学大学院保健学研究科保健学専攻

提出者氏名: 長 谷 川 和 輝

所 属: 放射線技術科学領域

指導教員: 細 川 洋 一 郎

目次

略語一覧

OSCC: 口腔扁平上皮癌 (oral squamous cell carcinoma)

RR: 放射線抵抗性 (radioresistant)

CSC: 癌幹細胞 (cancer stem cell)

HA: ヒアルロン酸 (hyaluronan)

EMT: 上皮間葉転換 (epithelial mesenchymal transition)

4-MU: 4-メチルウンベリフェロン (4-methylumbelliferone)

HAS: ヒアルロン酸合成酵素 (hyaluronan synthase)

IL: インターロイキン (interleukin)

NF-κB: 核内因子 κB (nuclear factor-kappa B)

SOD: スーパーオキシドジスムダーゼ (superoxide dismutase)

St-Hyal: ヒアルロン酸分解酵素 (*streptomyces* hyaluronidase)

PBS (-): リン酸緩衝液 (phosphate-buffered saline (-))

PE: フィコエリスリン (phycoerythrin)

CD: 分化抗原群 (cluster-of-differentiation)

FITC: フルオレセインイソチオシアナート (fluorescein isothiocyanate)

siRNA: 低分子干渉リボ核酸 (small interfering RNA)

HRP: 西洋ワサビペルオキシダーゼ (horseradish-peroxidase)

EGF: 上皮成長因子 (epidermal growth factor)

bFGF: 線維芽細胞成長因子 (basic fibroblast growth factor)

ELISA: 酵素結合免疫吸着検定法 (enzyme-linked immunosorbent assay)

IR: 2 Gy X 線照射 (2 Gy X-ray irradiation)

RT-qPCR: 定量的逆転写ポリメーラーゼ連鎖反応 (reverse transcription-quantitative polymerase chain reaction)

GAPDH: グリセルアルデヒド-3-リン酸デヒドロゲナーゼ (glyceraldehyde 3-phosphate dehydrogenase)

FSC: 前方散乱 (forward scatter)

SSC: 側方散乱 (side scatter)

ROS: 活性酸素種 (reactive oxygen species)

MFI: 平均蛍光強度 (mean fluorescence intensity)

DCFDA: ジクロロフルオレセインジアセテート (dichlorofluorescin diacetate)

PI3K: ホスファチジルイノシトール 3-キナーゼ (phosphoinositide 3-kinase)

LMW: 低分子量 (low molecular weight)

STAT3: シグナル伝達転写活性因子 3 (signal transducer and activator of transcription 3)

RHAMM: ヒアルロン酸媒介運動受容体 (receptor for hyaluronan-mediated motility)

TNF-α: 腫瘍壊死因子 (tumor necrosis factor-α)

序 論

Oral squamous cell carcinoma (OSCC) is a major malignant tumor of the head and neck that represents the 6th most common cancer worldwide and has shown an increasing trend in recent years [1, 2]. Besides surgery and chemotherapy, radiotherapy plays an important role in OSCC because it is non-invasive and provides good local control with the recent development of high-precision dose calculation techniques [3, 4]. Despite the advances in radiotherapy, the prognosis of patients with OSCC has not improved over the past 30 years [5, 6], and the acquisition of radioresistance during fractionated irradiation is considered one of the reasons for poor prognosis [7, 8]. In addition to OSCC, some other cancer cells have been reported to exhibit radioresistance during fractionated irradiation, such as non-small-cell lung and prostate cancer cells [9, 10]. Radioresistant (RR) cells remain after radiotherapy and cause recurrence and distant metastasis. Thus, they are a major concern associated with poor clinical outcomes [11-13]. Therefore, to improve the prognosis of patients with OSCC, it is important to establish strategies to sensitize RR cells.

Recently, in vitro RR cell models were established to understand their characteristics. Kuwahara et al. established clinically relevant RR cells via long-term fractionated X-ray irradiation and reported a higher repair capacity of DNA double-strand breaks in these cells compared with that of parental cancer cells [14]. Other studies have reported that RR cells have characteristics similar to those of cancer stem cells (CSCs), are more tumorigenic, and have enhanced anti-oxidant activity [15-17]. Therefore, although the mechanisms of radioresistance have been gradually elucidated, the underlying details are unclear, and effective radiosensitizers and clinical strategies are yet to be established.

Hyaluronan (HA), a major component of the extracellular matrix, is over-synthesized in cancer tissue and correlates with proliferation, invasion and epithelial mesenchymal transition (EMT), as well as metastasis [18-20]. The HA synthesis inhibitor 4-methylumbelliferone (4-MU) reduces the intracellular content of UDP-D-glucuronic acid [21-23]. In recent decades, 4-MU has been shown to exert anti-tumor and anti-invasive/-metastatic effects through suppressing HA synthase (HAS) expression in various cancer cells and mouse models [24, 25]. Furthermore, our previous studies

have indicated that 4-MU treatment with X-ray irradiation promotes anti-inflammatory effects by suppressing interleukin (IL) −6 and −1β, and intercellular communication (called non-targeted effects) involved in oxidative stress, and induces radiosensitizing effects [26-28]. Elevated expressions of IL-6 and nuclear factor-kappa B (NF-κB), a master regulator of the inflammatory response, have been suggested to enhance anti-apoptotic effect and production of superoxide dismutase (SOD) which is anti-oxidant enzyme in cancer cells and induce radioresistance [29-32]. Based on these findings, 4-MU is a potential radiosensitizer; however, it is unknown whether 4-MU administration radiosensitizes RR cells.

In this study, we used RR OSCC cell lines established via long-term fractionated X-ray irradiation and investigated, for the first time, the effect of 4-MU as a radiosensitizer.

方 法

Reagents. 4-MU (Nacalai Tesque, Kyoto, Japan) was diluted in dimethylsulfoxide (Fujifilm Wako Pure Chemical Industries, Ltd., Osaka, Japan) at a working concentration of 500 μM to minimize the cytotoxicity on normal fibroblasts and clearly observe the effects of 4-MU [26]. *Streptomyces* hyaluronidase (*St*-Hyal) (Seikagaku Corporation, Tokyo, Japan) was diluted in dH_2O and used at a final concentration of 100 TRU/mL. Calcium- and magnesium-free phosphate-buffered saline (PBS (-)) were purchased from Takara Bio Inc. (Otsu, Japan). Monoclonal phycoerythrin (PE)-conjugated anti-human cluster-of-differentiation (CD)-44 antibodies (cat. no. 338808), mouse monoclonal PE-IgG1, κ isotype control (cat. no. 400114), fluorescein isothiocyanate (FITC)-conjugated anti-human CD24 antibodies (cat. no. 311103), and mouse monoclonal FITC-IgG1 κ isotype control (cat. no. 400207) were obtained from BioLegend (San Diego, CA, USA). Small interfering RNA (siRNA) against HAS3 (sc-45295), the corresponding scrambled control siRNA (sc-37007), and anti-HAS3 (sc-365322) monoclonal primary antibodies were purchased from Santa Cruz Biotechnology, Inc. (Santa Cruz, CA, USA). Anti-β-actin (4970) monoclonal antibodies, anti-rabbit horseradish-peroxidase (HRP)-conjugated IgG (7074), and anti-mouse HRP-conjugated IgG (7076) secondary antibodies were purchased from Cell Signaling Technology (Tokyo, Japan). Epidermal growth factor (EGF) and basic fibroblast growth factor (bFGF) were purchased from Fujifilm Wako Pure Chemical, Ltd.

Cell Culture. The human OSCC cell lines HSC2 and HSC3, and their RR counterparts HSC2-R and HSC3-R, were obtained from the Cell Resource Center for Biomedical Research, Institute of Development, Aging and Cancer, Tohoku University. HSC2 and HSC3 cells were repeatedly fractionated X-ray irradiation at 2 Gy/day for 30 consecutive days, and cells that continued to proliferate after a total dose of more than 60 Gy were established as HSC2-R and HSC3-R cells, respectively [33]. RR cells were exposed to 2 Gy of X-rays every 24 hours to maintain radioresistant characteristics for more than one year. The cell lines were cultured in Roswell Park Memorial Institute 1640 medium (Thermo Fisher Scientific Inc., Waltham, MA, USA), supplemented with 10% heat-inactivated fetal bovine serum (FBS; Japan Bio Serum, Fukuyama, Japan) and 1% penicillin/streptomycin (Fujifilm Wako Pure Chemical Industries, Ltd.) and maintained at 37 °C and

in a 5% CO_2 environment.

Irradiation Condition. The cultured cells were irradiated using an X-ray generator (MBR-1520R-3; Hitachi Medical Co., Tokyo, Japan) as previously reported [27]. The total dose and dose rate of 1.0 Gy/min were measured using an ionizing chamber (MZ-BD-3, Hitachi Medical Co., Tokyo, Japan) placed next to the sample, and the dose rate in the air was determined by converting the air kerma.

SiRNA Transfection. Each cell line was seeded in φ60 mm culture dishes without antibiotics and incubated for 18 h. Samples were washed with PBS (-) and transfected with siRNA using Lipofectamine RNAiMAX (Invitrogen; Thermo Fisher Scientific, Inc.), following the manufacturer's instructions. The final concentration of both the siRNA and scrambled control siRNA was 50 nM, and the cells were harvested after transfection for 48 h.

HA Density Quantitation. The HA concentration in the culture supernatant was detected using a Hyaluronan Quantikine enzyme-linked immunosorbent assay (ELISA) kit (R&D Systems, Inc., Minneapolis, MN, USA), as reported previously [34]. The HA concentration was calculated from the standard curve of the absorbance measured at 450 nm.

Clonogenic Survival Assay. The clonogenic potency was evaluated via a colony formation assay. The appropriate number of cells was seeded on φ60 mm culture dishes and incubated for 2 h and subjected to 500 μM 4-MU or 100 TRU/mL *St*-Hyal with 2 Gy X-ray irradiation (IR). Given the cell-killing effects of each treatment, the cells were seeded in different numbers to form the appropriate number of colonies. After treatment for 24 h, 4-MU and *St*-Hyal were washed out, and the cells were further incubated for 7–10 days, fixed with methanol (Fujifilm Wako Pure Chemical Industries) and stained with a Giemsa staining solution (Fujifilm Wako Pure Chemical Industries). Colonies with >50 cells were counted. The surviving fraction for each cell line was calculated from the ratio of the plating efficiency of the irradiated and/or 4-MU- or *St*-Hyal-administrated samples with that of the control samples.

Monolayer Wound Healing Assay. Each cell line was plated and allowed to form a confluent monolayer, which was then scratched with the thin edge of a 200 μL microtip. Cell migration images at 0, 6, 12, and 24 h after treatment were obtained using an Olympus IX71 fluorescence microscope (Tokyo, Japan) and DP2-BSW software (Olympus) at 10× magnification. The wound distance was

measured at each time point, and the cell migration rates compared with those at 0 h were calculated. This was performed in three independent experiments.

RNA Extraction and Reverse Transcription-Quantitative Polymerase Chain Reaction (RT-qPCR). Total RNA was extracted from each sample, and cDNA synthesis was performed with a reaction mixture containing forward and reverse primers, as previously described [27]. RT-qPCR was performed using a real-time PCR system (StepOne Plus; Life Technologies, Waltham, MA, USA) with the following conditions: 95 °C for 30 s, followed by 40 cycles of 95 °C for 5 s and 54 °C for 30 s. Target gene expression levels were calculated relative to glyceraldehyde 3-phosphate dehydrogenase (GAPDH, internal control) mRNA via the comparative ΔΔCq method [35]. The following specific primer sequences were used: HAS1 (forward, 5′-TGTGTATCCTGCATCAGCGGT-3′; reverse, 5′-CTGGAGGTGTACTTGGTAGCATAACC-3′), HAS2 (forward, 5′-CTCCGGGACCACACAGAC-3′; reverse, 5′-TCAGGATACATAGAAACCTCTCACA-3′), HAS3 (forward, 5′-ACCATCGAGATGCTTCGAGT-3′; reverse, 5′-CCATGAGTCGTACTTGTTGAGG-3′), and GAPDH (forward, 5′-GTGAAGGTCGGAGTCAACG-3′; reverse, 5′-TGAGGTCAATGAAGGGGTC-3′).

Flow Cytometric Analysis. To evaluate the expression of HA receptor CD44 and CSC marker CD24, cells were stained with PE-conjugated anti-human CD44 antibodies (3 μL/10^6 cells) and FITC-conjugated anti-human CD24 antibodies (3 μL/10^6 cells) and analyzed using FACS Aria Cell Sorter (BD Biosciences, Ltd., Tokyo, Japan) according to previously reported procedures [26]. To perform the appropriate analysis, the following gating strategy was used to define the staining population: the targeted population was gated by forward and side scatter (FSC and SSC, respectively), and the doublets and debris were removed. The gating population was reflected in the dot plot, and 1% each of CD44 (+) and CD24 (+) were gated in the dot plot as isotype controls. This gate was adapted to each treatment group, and the expressions of CD44 and CD24 were evaluated. Oxidative stress (caused by reactive oxygen species (ROS)), which is intrinsically related to DNA damage induction, was measured via a dichlorofluorescin diacetate (DCFDA) assay (H2DCFDA, Cellular ROS Assay Kit, Abcam, Tokyo, Japan). The mean fluorescence intensity (MFI) of DCFDA

per cell was measured at 0, 2, and 24 h after treatments. DCFDA staining and 4-MU administration were simultaneously performed 30 min before irradiation. The increment of the ROS level at 0 h was similar to that observed in our previous report [28]. The gating strategy was similar to that of the CD44 and CD24 analyses; after removal of the doublets and debris gated on the target population based on FSC and SSC dot plots, this gating was reflected in the histogram of each treatment group, and the MFI of DCFDA was evaluated.

SDS-PAGE and Western Blotting. Harvested cells were lysed in 1× radioimmunoprecipitation (RIPA) buffer (Santa Cruz Biotechnology), mixed with 2 × volume gel electrophoresis loading buffer (Tis-Glycine sodium dodecyl sulfate (SDS)) containing 1.5% 2-mercaptoethanol (Fujifilm Wako Pure Chemicals Industries) and boiled at 100 °C for 5 min. The protein concentration was determined using a BCA protein assay kit (Takara Bio) and an iMark microplate reader (Bio-Rad Laboratories, Inc., Hercules, CA, USA). The proteins (~20 μg/lane) were separated using 5–20% EHR-520L e-PAGEL HR (ATTO, Tokyo, Japan) and were electro-transferred onto polyvinylidene difluoride (PVDF) membranes in 25 mM Tris/192 mM glycine, pH 8.3, at 25 V for 2 h. Membranes were blocked using EzBlock Chemi (ATTO) at room temperature for 1 h, and then incubated overnight with primary antibodies, anti-HAS3 (1:1000), and anti-actin antibodies (1:3000) at 4 °C. The membranes were then incubated with HRP-conjugated secondary antibodies in EzBlock Chemi at room temperature for 90 min. The following secondary antibodies were used: HRP-linked anti-rabbit IgG (1:5000) or HRP-linked anti-mouse IgG (1:5000). Antigens were visualized using a chemiluminescence Western blotting substrate (Bio-Rad Laboratories), and blot stripping was performed using a stripping solution (Fujifilm Wako Pure Chemical Industries).

Assay of SOD Activity. SOD activity in each sample was detected using a WST-SOD assay kit (Dojindo Molecular Technologies, Inc., Kumamoto, Japan) according to the manufacturer's instructions. Cells were harvested in PBS (-) and sonicated with 30 sec pulses (20% output control) on ice. The supernatants were collected after centrifugation of the cell lysate at 10,000× g for 15 min at 4 °C. The supernatants and WST-working solutions were added to each 96-well plate. The enzyme solution was pipetted into each well, and the plates were incubated at 37 °C for 20 min. Subsequently, SOD activity (expressed as unit/10^6 cells) was measured at 450 nm using an iMark microplate reader.

Statistical Analysis. Data are presented as mean ± SD of the three independent experiments. Comparisons between the control and experimental groups were performed using the two-sided Student's t-test or Mann–Whitney U-test depending on data distribution. Multiple comparisons were performed with the one-way analysis of variance, followed by the Tukey–Kramer test. Non-parametric tests were analyzed using Steel-Dwass test. Statistical significance was set at $p < 0.05$. Statistical analyses were performed using Microsoft Excel 2016 (Microsoft Corporation, Redmond, WA, USA) with Statcel v4 add-in software (OMS Publishing, Saitama, Japan).

結 果

Evaluation of the Effect of 4-MU on Radioresistance

We first confirmed the efficiency of 4-MU in RR cells. We evaluated the radiosensitization of RR cells treated with 4-MU and IR via a colony formation assay. The surviving fraction of 4-MU-treated cells was significantly lower than that of the control cells, and the combination of 4-MU and IR significantly suppressed the surviving fraction compared with IR alone (Figure 1A). On the other hand, the surviving fraction after IR in the control and 4-MU-treated cells did not change, respectively, with the exception of HSC2-R cells. These results suggested that 4-MU treatment enhances anti-tumor effects, but not radiosensitizing effects.

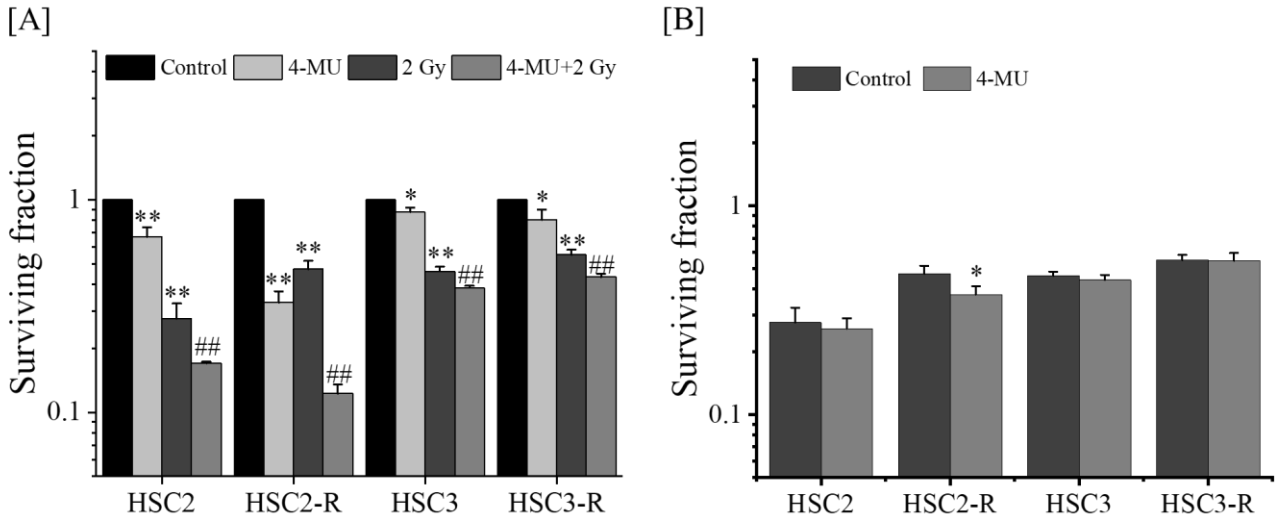

Figure 1. Logarithmic surviving fraction of each cell line treated with 4-methylumbelliferone (4-MU). (A) The cell surviving fraction of each cell line under 500 μM 4-MU and 2 Gy X-ray irradiation (IR); * and ** indicate $p < 0.05$ and $p < 0.01$ vs. control, respectively; ## indicates $p < 0.01$ vs. 2 Gy, respectively. (B) The cell surviving fraction after 2 Gy irradiation in the control and 4-MU treatment groups, respectively; * indicates $p < 0.05$ vs. control.

Next, we measured the cell migration ability via a wound healing assay. The cell migration rates were significantly inhibited in HSC2 and HSC2-R cells 12 h after 4-MU treatment and in HSC3 and HSC3-R cells 6 h after treatment compared with those of their controls (Figure 2A, B). We also evaluated cell migration following stimulation with EGF/bFGF. The cell migration rate 12 h after EGF/bFGF treatment was significantly enhanced compared with that of the controls; even under

these conditions, 4-MU treatment significantly suppressed cell migration (Figure 1B, C). These results indicated 4-MU contributes to the anti-metastatic effects in RR cells by inhibiting cell migration.

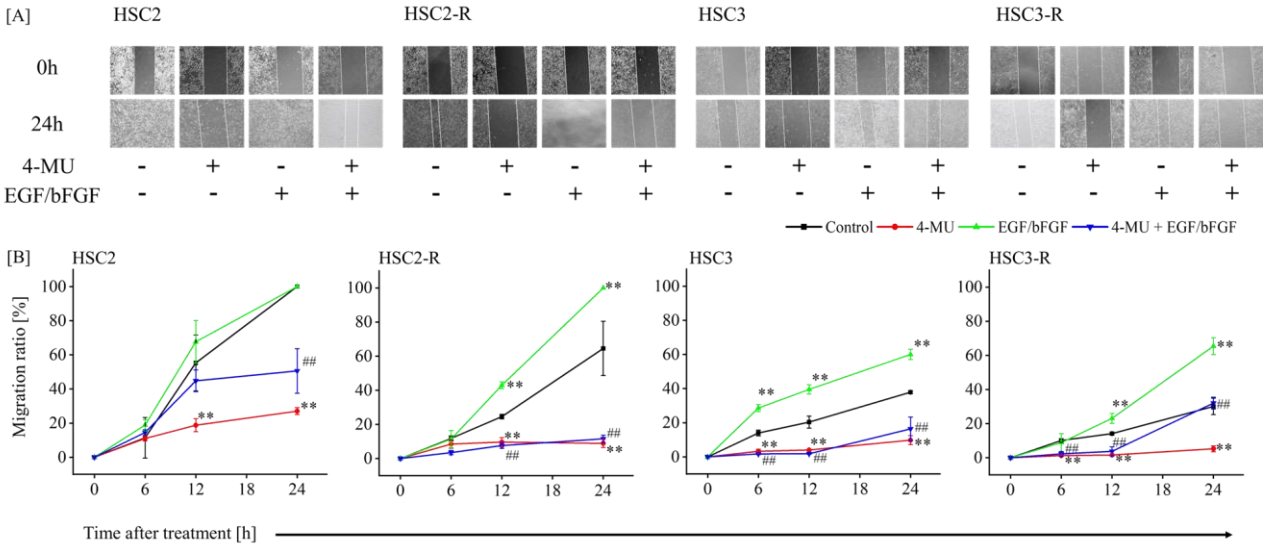

Figure 2. Wound healing assay treated with 4-MU. (A) Representative images of each cell line at 0 and 24 h after treatment with 4-MU and epidermal growth factor (EGF)/basic fibroblast growth factor (bFGF) stimulation. (B) Cell migration ratio at 0, 6, 12, and 24 h after treatment with 4-MU and EGF/bFGF stimulation; * and ** indicate $p < 0.05$ and $p < 0.01$ vs. control, respectively; ## indicates $p < 0.01$ vs. EGF/bFGF.

Investigation of Mechanisms of the cell killing effects with 4-MU

Next, we examined the mechanisms by which 4-MU enhances cell killing effects of RR cells. The expressions of CD44 and CD24 (CSC markers) were analyzed via flow cytometry. The ratio of the CD44 (+)/CD24 (-) fraction, which is used to assess the CSC-like phenotype of OSCC [36, 37], significantly decreased after 4-MU treatment compared with that of the controls (Figure 3A, B). In addition, this fraction was suppressed by IR treatment only in the HSC3-R cells. The MFI of CD44 was significantly suppressed through 4-MU treatment compared with that of the controls (Figure 3C). IR treatment showed a similar tendency to suppress the MFI of CD44, and the combination of 4-MU and IR significantly suppressed it compared with that of the controls. IR treatment did not affect the MFI of CD24, whereas the combination of 4-MU and IR significantly enhanced it compared with IR

alone (Figure 3D).

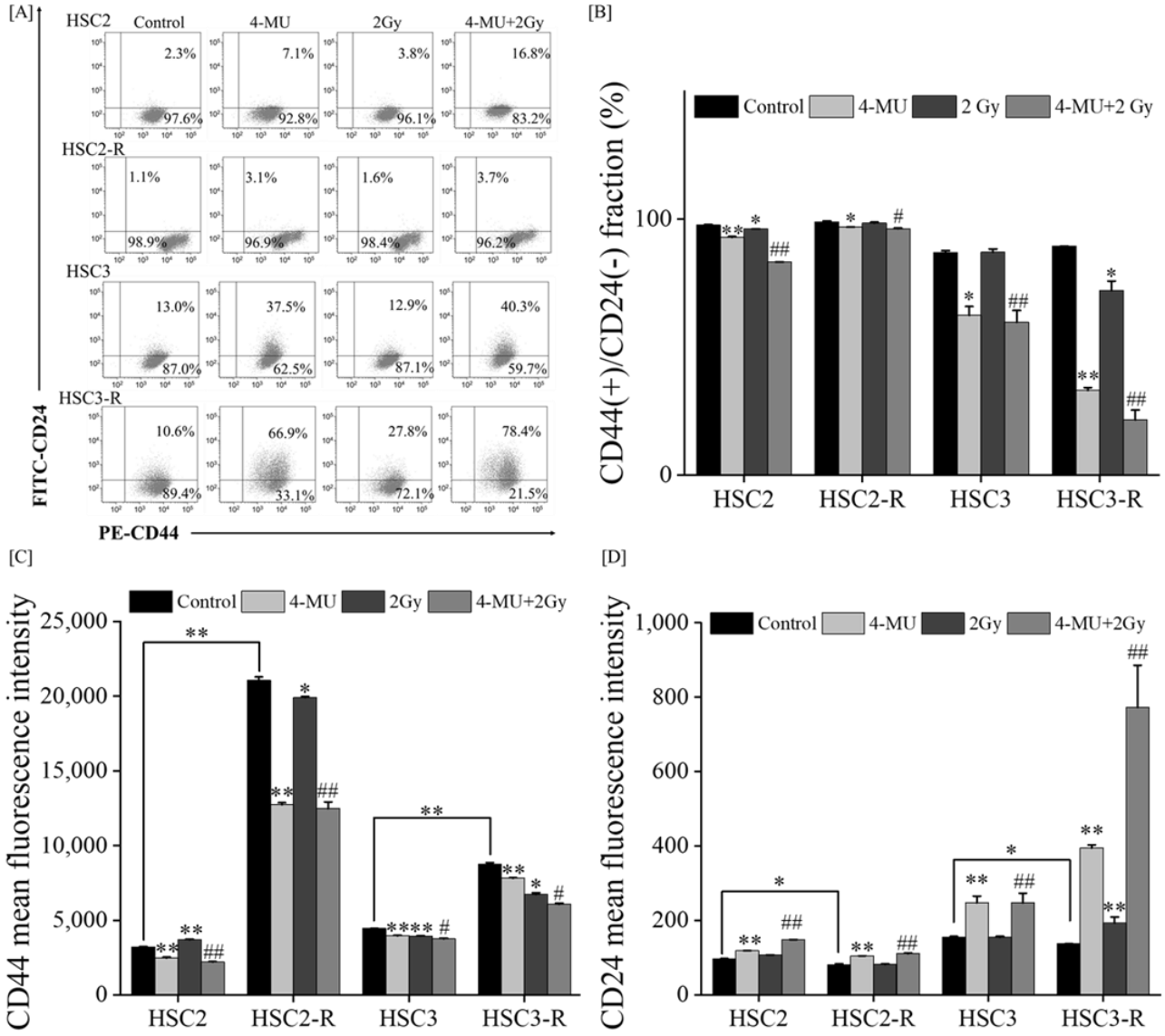

Figure 3. Cluster-of-differentiation (CD)-44 and CD24 expression measured via flow cytometry. (A) Representative cytograms of each cell line. (B) Cell populations of CD44 (+)/CD24 (-) irradiated with 2 Gy under 500 μM 4-MU. (C, D) Mean fluorescence intensity (MFI) of (C) CD44 or (D) CD24 irradiated with 2 Gy under 500 μM 4-MU; * and ** indicate $p < 0.05$ and $p < 0.01$ vs. control, respectively; # and ## indicate $p < 0.05$ and $p < 0.01$ vs. 2 Gy, respectively.

As CD44 and CD24 have been reported to contribute to anti-oxidant activity [38-40], we evaluated intracellular ROS levels following 4-MU administration. The intracellular ROS levels in HSC2-R and HSC3-R cells were significantly lower than those in their respective parental cells,

HSC2 and HSC3 (Figure 4A). The ROS level of the IR group did not change compared to that of the control group, while those of the 4-MU alone and combined groups significantly increased from 0 h, and the effects were sustained for 24 h after treatment (Figure 4B, C). Next, we measured the SOD production levels in the presence of 4-MU. The SOD levels in HSC2-R and HSC3-R cells were significantly higher than those in HSC2 and HSC3 cells, and IR treatment significantly enhanced SOD activity compared with the control (Figure 4D). The SOD level after 4-MU administration in HSC2-R and HSC3-R cells was significantly suppressed compared with that in their respective control groups, whereas in HSC2 and HSC3 cells, it remained unchanged or slightly increased. The combination of 4-MU and IR significantly suppressed the SOD levels compared with IR alone.

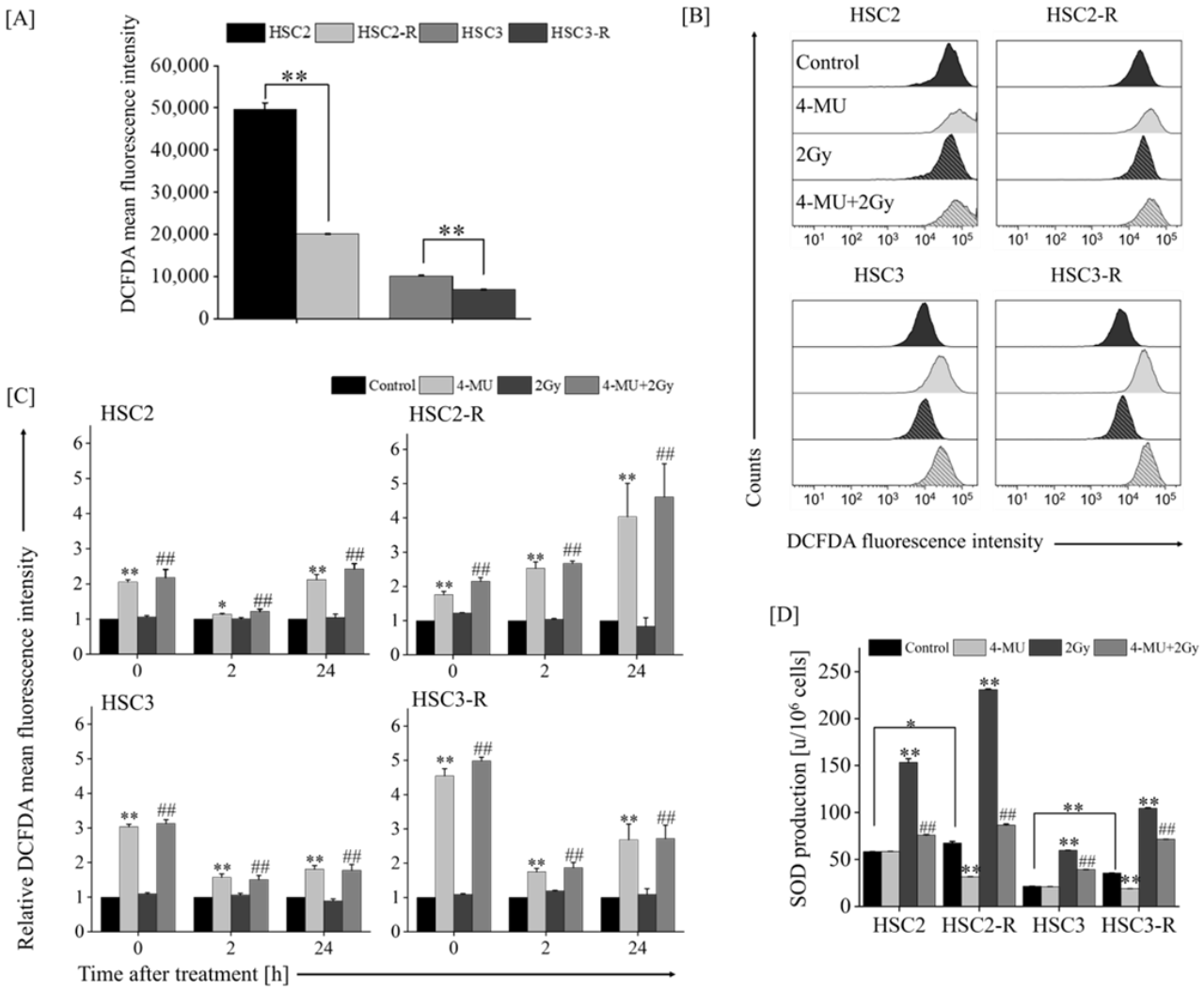

Figure 4. Oxidative stress levels measured via flow cytometry and a superoxide dismutase (SOD) assay. (A) Intracellular reactive oxygen species (ROS) levels in each of the control cells. (B)

Representative histograms of each cell line irradiated with 2 Gy under 500 μM 4-MU. (C) Relative intracellular ROS levels in each cell line at 0, 2, and 24 h after treatment. The MFI of IR alone, 500 μM 4-MU alone, and the combination (4-MU + IR) were standardized based on the MFI of the control group at each time. (D) SOD production levels of each cell line after treatment for 24 h; * and ** indicate $p < 0.05$ and $p < 0.01$ vs. control, respectively; ## indicates $p < 0.01$ vs. 2 Gy.

The Effects of Extracellular HA Elimination or HAS Inhibition on RR cells

As 4-MU is an HA synthesis inhibitor, we further investigated the cell killing effects of extracellular HA elimination via *St*-Hyal or HAS knockdown by using siRNA. First, as a concentration study for *St*-Hyal, the HA concentration in the cell culture supernatant 24 h after *St*-Hyal treatment was analyzed via ELISA. Because all tested concentrations showed measurement results below the detection limit, we detected the concentration of *St*-Hyal based on the results of other studies [41, 42]. We evaluated the effect of extracellular HA elimination on cell survival of RR cells via a colony formation assay. Surprisingly, the surviving fraction treated with *St*-Hyal did not change compared with their control cells, even though extracellular HA was completely eliminated (Figure 5).

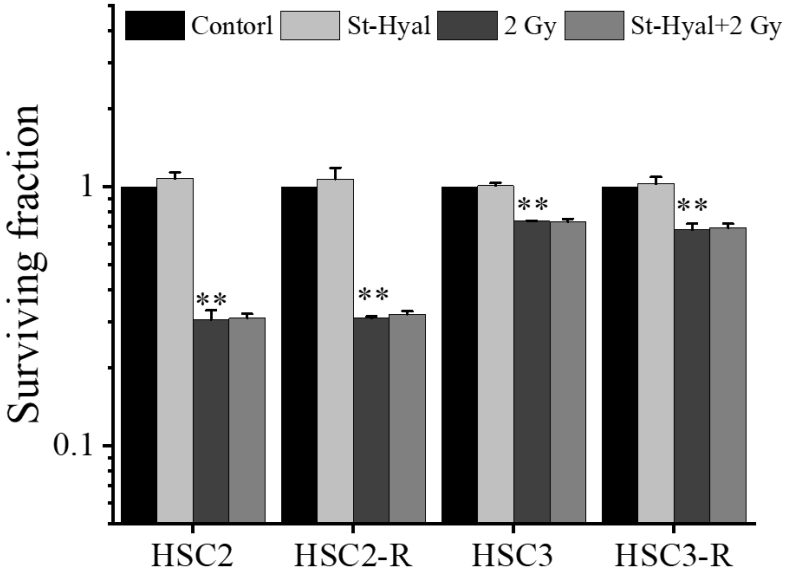

Figure 5. Logarithmic surviving fraction of each cell line treated with 100 TRU/mL *St*-Hyal and IR; ** indicates $p < 0.01$ vs. control, respectively.

Next, we investigated HAS expression and found that HAS1 mRNA expression was not detected, whereas HAS3 expression was significantly higher than HAS2 expression in the RT-qPCR analysis (Figure 6A). In addition, HAS3 expression in HSC2-R and HSC3-R cells was much higher than that in HSC2 and HSC3 cells, respectively, and 4-MU administration significantly suppressed HAS3 expression compared with that in the control cells (Figure 6B). Therefore, we suppressed HAS3 expression using siRNA, and the knockdown efficiency was confirmed by Western blotting (Figure 6C).

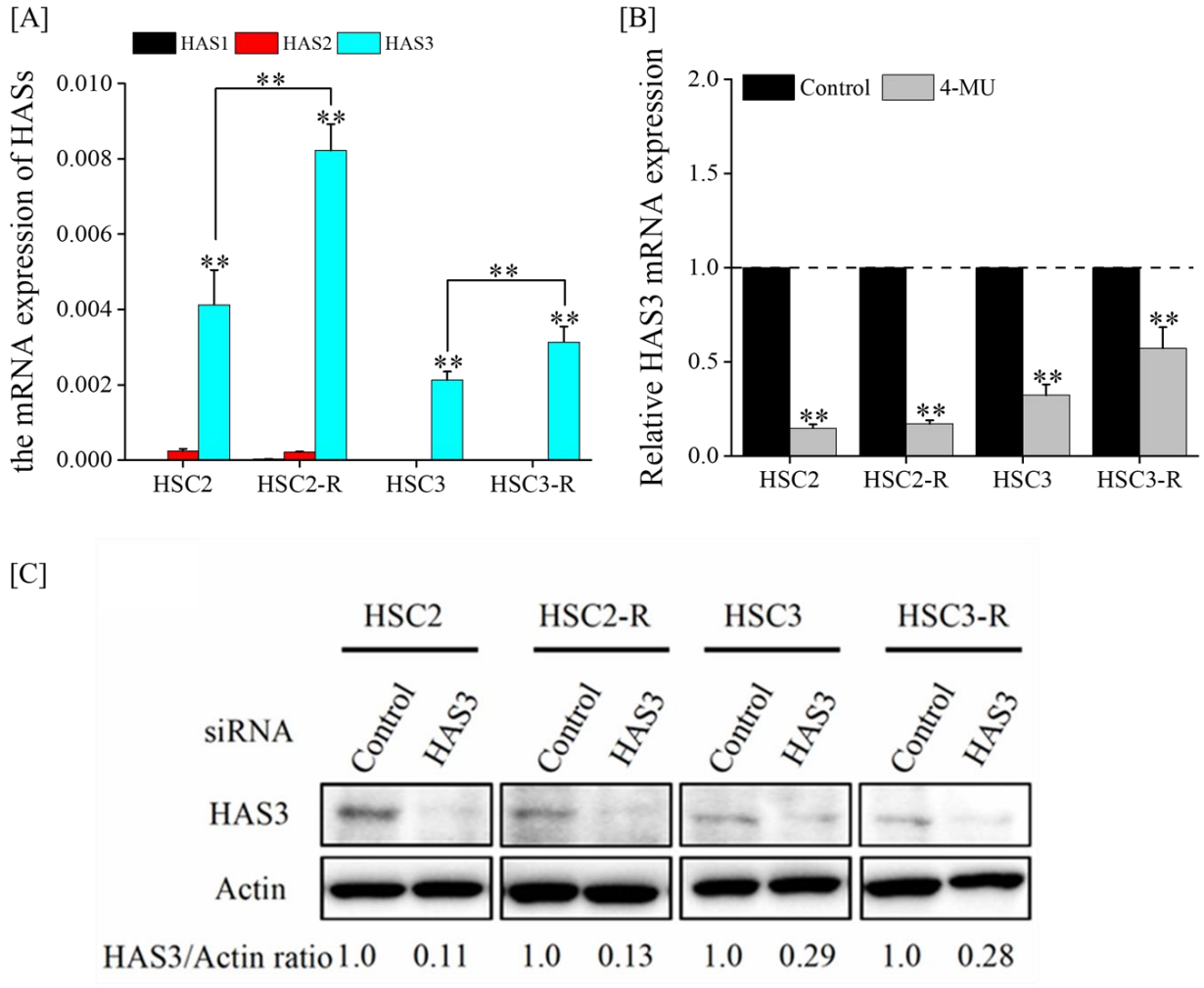

Figure 6. The mRNA expression of HAS as measured by RT-qPCR and the protein expression of HAS3 as measured by Western blotting. (A) mRNA expression of HAS in each cell line. (B) Relative mRNA expression of HAS3 treated with 500 μM 4-MU. ** indicates $p < 0.01$ vs. control. (C) Representative images of immunoblots are shown. Actin was used as a loading control, and the relative values of the HAS3/actin ratio are presented. For the HAS3 proteins, both bands were

quantified together.

Next, we evaluated the effect of HAS3 knockdown on cell survival via a colony formation assay. The surviving fraction of HAS3 knockdown cells was significantly lower than that of the control cells, and the combination of HAS3 knockdown and IR significantly suppressed the surviving fraction compared with IR alone (Figure 7A). Moreover, the surviving fraction after IR in the HAS3knockdown cells was significantly lower than those of their control cells respectively (Figure 7B). These results suggested that HAS3 knockdown not only enhances anti-tumor effects, but also radiosensitizing effects.

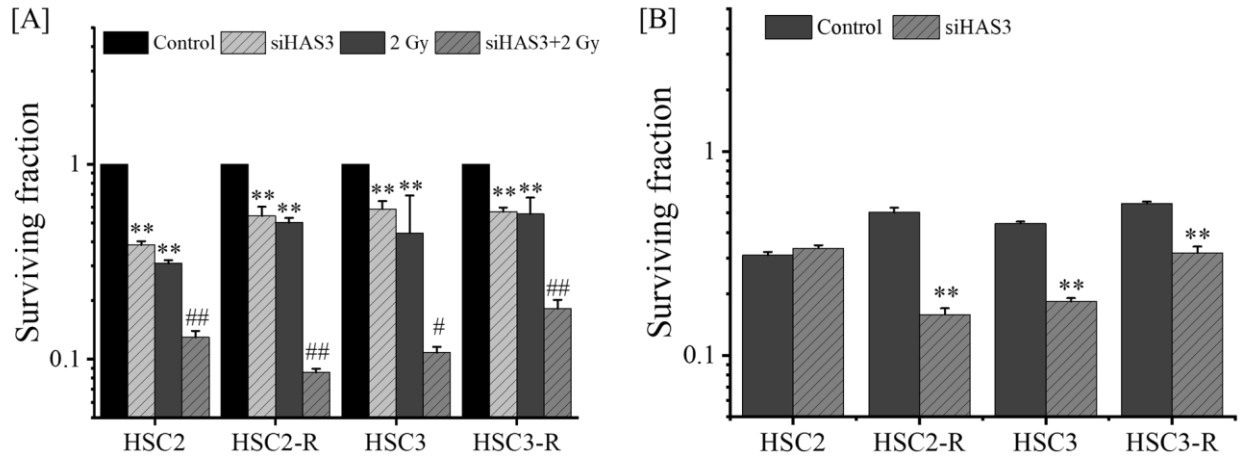

Figure 7. Effects of HAS3 knockdown on RR cells. (A) Logarithmic surviving fraction of each cell line treated with HAS3 knockdown and IR; * and ** indicate $p < 0.05$ and $p < 0.01$ vs. control, respectively; $^{\#}$ and $^{\#\#}$ indicate $p < 0.05$ and 0.01 vs. 2 Gy, respectively. (B) The cell surviving fraction after 2 Gy irradiation in the control and HAS3 knockdown groups, respectively; ** indicates $p < 0.01$ vs. control.

Similar to 4-MU treatment, the ratio of the CD44 (+)/CD24 (-) fraction significantly decreased by HAS3 knockdown compared with that of the controls (Figure 8A, B). In addition, the MFI of CD44 was significantly suppressed and CD24 was significantly increased via HAS3 knockdown compared with that of the controls (Figure 8C, D). The SOD levels were inhibited through HAS3 knockdown, and co-treatment (HAS3 knockdown and IR) significantly suppressed SOD levels compared with the IR treatment alone (Figure 8E). These results suggested that HAS3

knockdown has similar effects to 4-MU administration and that HAS3 may be an important factor for radiosensitization.

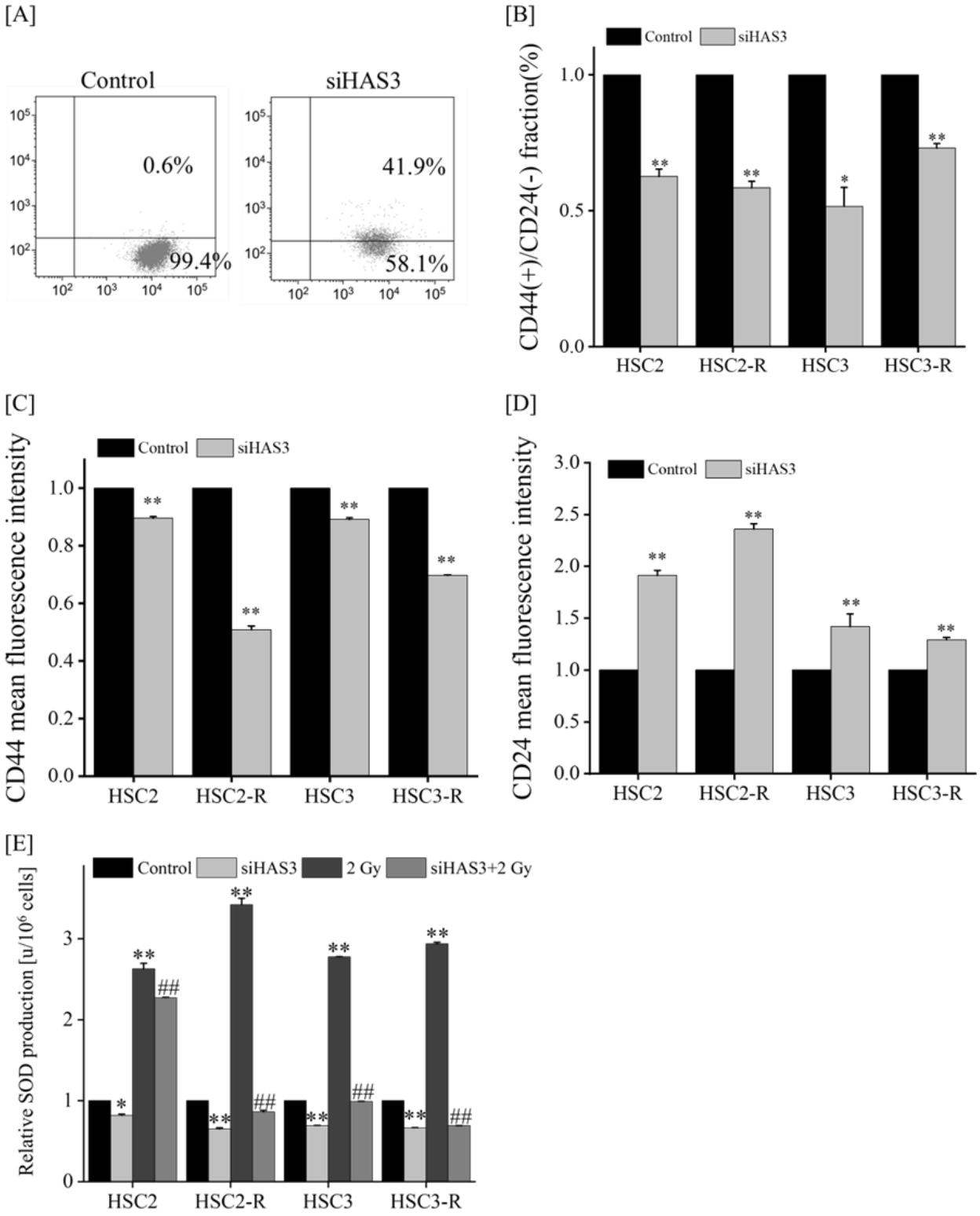

Figure 8. Effects of HAS3 knockdown on CD44 and CD24 expression and SOD production levels. (A) Representative cytograms of HAS3 knockdown. (B) Cell populations of CD44 (+)/CD24 (-)

treated with HAS3 knockdown. (C, D) Mean fluorescence intensity (MFI) of (C) CD44 or (D) CD24 treated with HAS3 knockdown. (E) Relative SOD production levels of each cell line treated with HAS3 knockdown and IR. The SOD production levels of IR alone, HAS3 knockdown, and combined treatment groups were standardized based on the SOD level of the control group; * and ** indicate $p < 0.05$ and $p < 0.01$ vs. control, respectively; $^{\#}$ and $^{\#\#}$ indicate $p < 0.05$ and $p < 0.01$ vs. 2 Gy, respectively.

考 察

The anti-tumor effects of 4-MU and the role of HAS in various malignancies have been reported [43-45]. Our previous studies revealed the enhancement of anti-inflammatory effects and the suppression of anti-oxidant activity by 4-MU [26-28]. However, it remains unclear whether 4-MU has radiosensitizing effects on RR cells. Our results demonstrated that 4-MU treatment with IR significantly suppressed cell survival compared with IR alone (Figure 1A), and 4-MU administration significantly suppressed cell migration compared with EGF/bFGF (Figure 2A, B,). On the other hand, there are no significance between the cell survival after IR in the control and 4-MU-treated cells (Figure 1B). These results suggested that 4-MU may exert anti-tumor and anti-metastatic effects on RR cells, but not induce radiosensitizing effects. In addition, 4-MU treatment significantly suppressed the CD44 (+)/CD24 (-) ratio and similarly significantly suppressed the MFI of CD44 and significantly enhanced the MFI of CD24 (Figure 3). In OSCC cell lines, the CD44 (+)/CD24 (-) fraction has been reported in CSC-like cells [36, 37]. CD44 stabilizes xCT, a cystine–glutamate transporter that contributes to glutathione (GSH) synthesis for ROS defense on the cell surface, leading to redox regulation in several cancers [40, 46, 47]. It was also reported that CD24 expression correlates the ROS levels, and its elevated expression suppresses NF-κB signaling and enhances oxidative stress through ROS enhancement in the CD44 (+)/CD24 (-) phenotype of breast cancer [38, 48, 49]. Moreover, the HA/CD44 interaction was reported to promote inflammatory cytokines [50]; specifically, IL-1β induces human manganese SOD genes such as *SOD2*, which encodes an enzyme that degrades reactive oxygen generated in cells [51]. Our previous study also indicated that 4-MU treatment inhibits the production of IL-1β and IL-6 [26]. The results of this study showed that 4-MU treatment enhanced the intracellular ROS levels and suppressed SOD production (Figure 4). As ROS levels were not affected by IR treatment, the combination of 4-MU and IR showed similar effects as 4-MU treatment alone, whereas SOD production was significantly increased by IR treatment compared with that in the control, and the combination of 4-MU and IR significantly suppressed SOD production compared with IR alone (Figure 4C, D). These results suggested that 4-MU dose not induce the radiosensitizing effects on RR cells, while it can effectively suppress RR cells by enhancing their anti-tumor effect through the CSC phenotype suppression and oxidative stress

enhancement.

Since 4-MU is an HA synthesis inhibitor, a further upstream mechanistic analysis was performed to investigate its cell killing effects by eliminating extracellular HA using *St*-Hyal or via siRNA-based HAS3 knockdown. Because the HA-binding domain of CD44 is present in the extracellular space, extracellular HA is predominantly used in HA/CD44 interactions [52]. In this study, *St*-Hyal treatment completely removed extracellular HA, but did not affect the cell survival and also did not induce radiosensitizing effect (Figure 5), whereas HAS3 knockdown by siRNA significantly suppressed the cell survival and induced radiosensitizing effects on RR cells (Figure 7). Moreover, HAS3 knockdown treatment had similar effects to 4-MU treatment on CSC phenotype ratio, CD44 and CD24 expression (Figure 8). The HA/CD44 interaction promotes CD44/phosphoinositide 3-kinase (PI3K) complex formation and activates the downstream Akt pathway related to cell survival and anti-apoptosis [53]. Moreover, Akt activation upregulates CD44 expression, which further enhances HA/CD44 interaction (feedback loop) [25]. It was also reported that HAS3 accounts for most of the HA synthesis in OSCC cells [54]. In addition, it is possible that *St*-Hyal treatment only eliminated extracellular HA but continued to supply HA through HAS, thereby maintaining the anti-oxidant effect of CD44 and the CSC-like phenotype. Therefore, it is suggested that elimination of extracellular HA only is not sufficient for cell killing effects and that inhibition of HA synthesis, particularly by HAS3, may disrupt the feedback loop of the interaction, and enhance the radiosensitizing effects.

Given that eliminating extracellular HA did not affect radiosensitization and that HAS releases HA into the intracellular space [55-57], it is possible that the intracellular HA synthesized by HAS3 is involved in radiosensitization. The HA synthesized by HAS3 has a low molecular weight (LMW), and the interaction between LMW-HA and CD44 has been reported to promote pro-oncogenic cellular actions [58, 59]. Although the HA binding site of CD44 is found in the extracellular space, it was recently reported that CD44 migrates into the nucleus and forms a complex with the signal transducer and activator of transcription 3 (STAT3), which induces cyclin D1 expression and promotes cell proliferation [60]. Therefore, it is possible that intracellular HA and CD44 interact [61]. Furthermore, the receptor for hyaluronan-mediated motility (RHAMM), another

major receptor for HA, is known to interact both intracellularly and at the plasma membrane [62-64] and was shown to promote tumorigenesis by binding to intracellular HA [65]. Kuo et al. also found that HAS3 and tumor necrosis factor (TNF)-α form an inter-regulatory loop in oral cancer cells [66] and that TNF-α promotes the enrichment of NF-κB to the HAS3 promoter region [67]. These findings suggest that interactions with intracellular HA synthesized by HAS3 or the direct action of HAS3 cause radioresistance. However, the role of intracellular HA is not fully understood and requires further investigation.

In conclusion, we showed for the first time that 4-MU treatment is not sufficient to induce radiosensitizing effects on RR cells, while targeting HAS3 may induce radiosensitizing effects via oxidative stress enhancement and CSC inhibition.

謝 辞

This work was supported by the Japan Society for the Promotion of Science (grant numbers: 19K08141 and 20K16814) and the JST SPRING (grant number JPMJSP2152). The funders had no role in the study design data collection and analysis, decision to publish, or preparation of the manuscript.

引用文献

1) Siegel R.L., Miller K.D., Jemal A. Cancer Statistics, 2017. *CA Cancer J. Clin*, 67: 7–30, 2017. doi: 10.3322/caac.21387.

2) Bray F., Ferlay J., Soerjomataram I., Seigel R.L., Torre L.A., Jemal A. Global cancer statistics 2018: GLOBOCAN estimates of incidence and mortality worldwide for 36 cancers in 185 countries. *CA Cancer Clin*, 68: 394–424, 2018. doi: 10.3322/caac.21492.

3) Narita Y., Kato T., Ono T., Oyama S., Komori S., Arai K., Abe Y., Harada T., Nakamura T., Wada H., et al. Effect of anatomical change on dose distribution during radiotherapy for maxillary sinus carcinoma: Passive scattering proton therapy versus volumetric-modulated arc therapy. *Br. J. Radiol*, 92: 20180273, 2018. doi: 10.1259/bjr.20180273.

4) Pfister D.G., Spencer S., Adelstein D., Adkins D., Anzai Y., Brizel D.M., Bruce J.Y., Busse P.M., Caudell J.J., Cmelak A.J., et al. Head and Neck Cancers, Version 2.2020, NCCN Clinical Practice Guidelines in Oncology. *J. Natl. Compr. Canc. Netw*, 18: 873–898, 2020. doi: 10.6004/jnccn.2020.0031.

5) Ou D., Blanchard P., El Khoury C., De Felice F., Even C., Levy A., Nguyen F., Janot F., Gorphe P., Deutsch E., et al. Induction chemotherapy with docetaxel, cisplatin and fluorouracil followed by concurrent chemoradiotherapy or chemoradiotherapy alone in locally advanced non-endemic nasopharyngeal carcinoma. *Oral Oncol*, 62: 114–121, 2016. doi: 10.1016/j.oraloncology.2016.10.011.

6) Tangthongkum M., Kirtstreesakul V., Supanimitjaroenporn P., Leelasawatsuk P. Treatment outcome of advance staged oral cavity cancer: Concurrent chemoradiotherapy compared with primary surgery. *Eur. Arch. Otorhinolaryngol*, 274: 2567–2572, 2017. doi: 10.1007/s00405-017-4540-9.

7) Bonner J.A., Harari P.M., Giralt J., Azarnia N., Shin D.M., Cohen R.B., Jones C.U., Sur R., Raben D., Jassem J., et al. Radiotherapy plus cetuximab for squamous-cell carcinoma of the head and neck. *N. Engl. J. Med*, 354: 567–678, 2006. doi: 10.1056/NEJMoa053422.

8) Shahinas J., Hysi D. Methods and risk of bias in molecular marker prognosis studies in oral

squamous cell carcinoma. *Oral Dis*, 24: 115–119, 2018. doi: 10.1111/odi.12753.

9) McDermott N., Meunier A., Mooney B., Nortey G., Hernandez C., Hurley S., Lynam-Lennon N., Baesoom S.H., Bowman K.J., Marples B., et al. Fractionated radiation exposure amplifies the radioresistant nature of prostate cancer cells. *Sci. Rep*, 6: 34796, 2016. doi: 10.1038/srep34796.

10) Arechaga-Ocampo E., Lopez-Camarillo C., Villegas-Sepulveda N., Gonzalez-De la Rosa C.H., Perez-Añorve I.X., Roldan-Perez R., Flores-Perez A., Peña-Curiel O., Angeles-Zaragoza O., Rangel Corona R., et al. Tumor suppressor miR-29c regulates radioresistance in lung cancer cells. *Tumor Biol*, 39: 1010428317695010, 2017. doi: 10.1177/1010428317695010.

11) Hara T., Iwadate M., Tachibana K., Waguri S., Takenoshita S., Hamada N. Metastasis of breast cancer cells to the bone, lung, and lymph nodes promotes resistance to ionizing radiation. *Strahlenther. Onkol*, 193: 848–855, 2017. doi: 10.1007/s00066-017-1165-2.

12) Kim J.S., Chang J.Y., Yun S.H., Yang K.M., Hong E.H., Kim D.H., Um H.D., Lee K.H., Lee S.J., Hwang S.G. Chloride intracellular channel 1 identified using proteomic analysis plays an important role in the radiosensitivity of Hep-2 cells via reactive oxygen species production. *Proteomics*, 10: 2589–2604, 2010. doi: 10.1002/pmic.200900523.

13) Jin Y., Xu K., Chen Q., Wang B., Pan J., Huang S., Wei Y., Ma H. Simvastatin inhibits the development of radioresistant esophageal cancer cells by increasing the radiosensitivity and reversing EMT process via the PTEN-PI3K/AKT pathway. *Exp. Cell Res*, 362: 362–369, 2018. doi: 10.1016/j.yexcr.2017.11.037.

14) Kuwahara Y., Li L., Baba T., Nakagawa H., Shimura T., Yamamoto Y., Ohkubo Y., Fukumoto M. Clinically relevant radioresistant cells efficiently repair DNA double-strand breaks induced by X-rays. *Cancer Sci*, 100: 747–752, 2009. doi: 10.1111/j.1349-7006.2009.01082.x.

15) Nagano O., Okazaki S., Saya H. Redox regulation in stem-like cancer cells by CD44 variant isoforms. *Oncogene*, 32: 5191–5198, 2013. doi: 10.1038/onc.2012.638.

16) Alshareeda A.T., Negm O.H., Albarakati N., Green A.R., Nolan C., Sultana R., Madhusudan S., Benhasouna A., Tighe P., Ellis I.O., et al. Clinicopathological significance of KU70/KU80, a key DNA damage repair protein in breast cancer. *Breast Cancer Res. Treat*, 139: 301–310, 2013. doi: 10.1007/s10549-013-2542-x.

17) Groselj B., Kerr M., Kiltie A.E. Radiosensitisation of bladder cancer cells by panobinostat is modulated by Ku80 expression. *Radiother. Oncol*, 108: 429–433, 2013. doi: 10.1016/j.radonc.2013.06.021.

18) Kosaki R., Watanabe K., Yamaguchi Y. Overproduction of hyaluronan by expression of the hyaluronan synthase Has2 enhances anchorage-independent growth and tumorigenicity. *Cancer Res*, 59: 1141–1145, 1999.

19) Itano N., Sawai T., Miyaishi O., Kimata K. Relationship between hyaluronan production and metastatic potential of mouse mammary carcinoma cells. *Cancer Res*, 59: 2499–2504, 1999.

20) Jacobson A., Rahmanian M., Rubin K., Heldin P. Expression of hyaluronan synthase 2 or hyaluronidase 1 differentially affect the growth rate of transplantable colon carcinoma cell tumors. *Int J Cancer*, 102: 212–219, 2002. doi: 10.1002/ijc.10683.

21) Nakamura T., Takagaki K., Shibata S., Tanaka K., Higuchi T., Endo M. Hyaluronic-acid-deficient extracellular matrix induced by addition of 4-methylumbelliferone to the medium of cultured human skin fibroblasts. *Biochem. Biophys. Res. Commun*, 208: 470–475, 1995. doi: 10.1006/bbrc.1995.1362.

22) Kuroda Y., Kasai K., Nanashima N., Nozaka H., Nakano M., Chiba M., Yoneda M., Nakamura T. 4-Methylumbelliferone inhibits the phosphorylation of hyaluronan synthase 2 induced by 12-O-tetradecanoyl-phorbol-13-acetate. *Biomed. Res*, 34: 97–103, 2013. doi: 10.2220/biomedres.34.97.

23) Kultti A., Pasonen-Seppanen S., Jauhiainen M., Rilla K.J., Karna R., Pyoria E., Tammi R.H., Tammi M.I. 4-methylumbelliferone inhibits hyaluronan synthesis by depletion of cellular UDP-glucuronic acid and downregulation of hyaluronan synthase 2 and 3. *Exp. Cell Res*, 315: 1914–1923, 2009. doi: 10.1016/j.yexcr.2009.03.002.

24) Yates T.J., Lopez L.E., Lokeshwar S.D., Ortiz N., Kallifatidis G., Jordan A., Hoye K., Altman N., Lokeshwar V.B. Dietary supplement 4-methylumbelliferone: An effective chemopreventive and therapeutic agent for prostate cancer. *J. Natl. Cancer Inst*, 107: djv085, 2015. doi: 10.1093/jnci/djv085.

25) Piccioni F., Fiore E., Bayo J., Atorrasagasti C., Peixoto E., Rizzo M., Malvicini M.,

Tirado-González I., García M.G., Alaniz L., et al. 4-methylumbelliferone inhibits hepatocellular carcinoma growth by decreasing IL-6 production and angiogenesis. *Glycobiology*, 25: 825–835, 2015. doi: 10.1093/glycob/cwv023.

26) Saga R., Hasegawa K., Murata K., Chiba M., Nakamura T., Okumura K., Tsuruga E., Hosokawa Y. Regulation of radiosensitivity by 4-methylumbelliferone via the suppression of interleukin-1 in fibrosarcoma cells. *Oncol. Lett*, 14: 3555–3561, 2019. doi: 10.3892/ol.2019.9990.

27) Hasegawa K., Saga R., Takahashi R., Fukui R., Chiba M., Okumura K., Tsuruga E., Hosokawa Y. 4-methylubelliferone inhibits clonogenic potency by suppressing high molecular weight-hyaluronan in fibrosarcoma cells. *Oncol. Lett*, 19: 2801–2808, 2020. doi: 10.3892/ol.2020.11370.

28) Saga R., Matsuya Y., Takahashi R., Hasegawa K., Date H., Hosokawa Y. 4-Methylumbelliferone administration enhances radiosensitivity of human fibrosarcoma by intercellular communication. *Sci. Rep*, 11: 8258, 2021. doi: 10.1038/s41598-021-87850-3.

29) Guo G., Yan-Sanders Y., Lyn-Cook B.D., Wang T., Tamae D., Ogi J., Khaletskiy A., Li Z., Weydert C., Longmate J.A., et al. Manganese Superoxide Dismutase-Mediated Gene Expression in Radiation-Induced Adaptive Responses. *Mol. Cell Biol*, 23: 2362–2378, 2003. doi: 10.1128/MCB.23.7.2362-2378.2003.

30) Murley J.S., Kataoka Y., Cao D., Li J.J., Oberley L.W., Grdina D.J. Delayed radioprotection by NFkappaB-mediated induction of Sod2 (MnSOD) in SA-NH tumor cells after exposure to clinically used thiol-containing drugs. *Radiat. Res*, 162: 536–546, 2004. doi: 10.1667/RR3256.

31) Piao L., Canguo Z., Wenjie L., Xiaoli C., Wenli S., Li L. Lipopolysaccharides-stimulated macrophage products enhance Withaferin: A-induced apoptosis via activation of caspases and inhibition of NF-κB pathway in human cancer cells. *Mol. Immunol*, 81: 92–101, 2017. doi: 10.1016/j.molimm.2016.10.010.

32) Yu H., Aravindan N., Xu J., Natarajan M. Inter- and intra-cellular mechanism of NF-kB-dependent survival advantage and clonal expansion of radio-resistant cancer cells. *Cell Signal*, 31: 105–111, 2017. doi: 10.1016/j.cellsig.2017.01.011.

33) Kuwahara Y., Mori M., Oikawa T., Shimura T., Ohtake Y., Mori S., Ohkubo Y., Fukumoto M.

The modified high-density survival assay is the useful tool to predict the effectiveness of fractionated radiation exposure. *J. Radiat. Res*, 51: 297–302, 2010. doi: 10.1269/jrr.09094.

34) Saga R., Monzen S., Chiba M., Yoshino H., Nakamura T., Hosokawa Y. Anti-tumor and anti-invasion effects of a combination of 4-methylumbelliferone and ionizing radiation in human fibrosarcoma cells. *Oncol. Lett*, 13: 410–416, 2017. doi: 10.3892/ol.2016.5385.

35) Liu Y.Y., Lee C.H., Dedaj R., Zhao H., Mrabat H., Sheidlin A., Syrkina O., Huang P.M., Garg H.G., Hales C.A., et al. High-molecular-weight hyaluronan—A possible new treatment for sepsis-induced lung injury: A preclinical study in mechanically ventilated rats. *Crit. Care*, 12: R102, 2008. doi: 10.1186/cc6982.

36) Todoroki K., Ogasawara S., Akiba J., Nakayama M., Naito Y., Seki N., Kusukawa J., Yano H. CD44v3+/CD24− cells possess cancer stem cell-like properties in human oral squamous cell carcinoma. *Int. J. Oncol*, 48: 99–109, 2016. doi: 10.3892/ijo.2015.3261.

37) Ghuwalewala S., Ghatak D., Das P., Dey S., Sarkar S., Alam N., Panda C.K., Roychoudhury S. CD44(high)CD24(low) molecular signature determines the Cancer Stem Cell and EMT phenotype in Oral Squamous Cell Carcinoma. *Stem Cell Res*, 16: 405–417, 2016. doi: 10.1016/j.scr.2016.02.028.

38) Bensimon J., Biard D., Paget V., Goislard M., Morel-Altmeyer S., Konge J., Chevillard S., Lebeau J. Forced extinction of CD24 stem-like breast cancer marker alone promotes radiation resistance through the control of oxidative stress. *Mol. Carcinog*, 55: 245–254, 2016. doi: 10.1002/mc.22273.

39) Schieber M.S., Chandel N.S. ROS links glucose metabolism to breast cancer stem cell and EMT phenotype. *Cancer Cell*, 23: 265–267, 2013. doi: 10.1016/j.ccr.2013.02.021.

40) Ishimoto T., Nagano O., Yae T., Tamada M., Motohara M., Oshima H., Ikeda T., Asaba R., Yagi H., Masuko T., et al. CD44 variant regulates redox status in cancer cells by stabilizing the xCT subunit of system xc(-) and thereby promotes tumor growth. *Cancer Cell*, 19: 387–400, 2011. doi: 10.1016/j.ccr.2011.01.038.

41) Nakamura T., Ishikawa T., Nanashima N., Miura T., Nozaka H., Nakaoka R., Sato T. 4-Methylumbelliferone induces the expression of membrane type 1-matrix metalloproteinase in

cultured human skin fibroblasts. *Biochem. Biophys. Res. Commun*, 298: 646–650, 2002. doi: 10.1016/S0006-291X(02)02516-0.

42) Yamada K. The effect of digestion with Streptomyces hyaluronidase upon certain histochemical reactions of hyaluronic acid-containing tissues. *J. Histochem. Cytochem*, 21: 794–803, 1973. doi: 10.1177/21.9.794.

43) Lokeshwar V.B., Lopez L.E., Munoz D., Chi A., Shirodkar S.P., Lokeshwar S.D., Escudero D.O., Dhir N., Altman N. Antitumor activity of hyaluronic acid synthesis inhibitor 4-methylumbelliferone in prostate cancer cells. *Cancer Res*, 70: 2613–2623, 2010. doi: 10.1158/0008-5472.CAN-09-3185.

44) Arai E., Nishida Y., Wasa J., Urakawa H., Zhuo L., Kimata K., Kozawa E., Futamura N., Ishiguro N. Inhibition of hyaluronan retention by 4-methylumbelliferone suppresses osteosarcoma cells in vitro and lung metastasis in vivo. *Br. J. Cancer*, 105: 1839–1849, 2011. doi: 10.1038/bjc.2011.459.

45) Urakawa H., Nishida Y., Wasa J., Arai E., Zhuo L., Kimata K., Kozawa E., Futamura N., Ishiguro N. Inhibition of hyaluronan synthesis in breast cancer cells by 4-methylumbelliferone suppresses tumorigenicity in vitro and metastatic lesions of bone in vivo. *Int. J. Cancer*, 130: 454–466, 2012. doi: 10.1002/ijc.26014.

46) Thanee M., Loilome W., Techasen A., Sugihara E., Okazaki S., Abe S., Ueda S., Masuko T., Namwat N., Khuntikeo N., et al. CD44 variant-dependent redox status regulation in liver fluke-associated cholangiocarcinoma: A target for cholangiocarcinoma treatment. *Cancer Sci*, 107: 991–1000, 2016. doi: 10.1111/cas.12967.

47) Bannai S., Ishii T. Transport of cystine and cysteine and cell growth in cultured human diploid fibroblasts, effect of glutamate and homocysteate. *J. Cell Physiol*, 112: 265–272, 1982. doi: 10.1002/jcp.1041120216.

48) Bontemps I., Lallemand C., Biard D., Dechamps N., Kortuewski T., Bourneuf E., Siberchicot C., Boussin F., Chevillard S., Campalans A., Lebeau J. Loss of CD24 promotes radiation- and chemo-resistance by inducing stemness properties associated with a hybrid E/M state in breast cancer cells. *Oncol Rep*, 49: 4, 2023. doi: 10.3892/or.2022.8441.

49) Ju J.H., Jang K., Lee K.M., Kim M., Kim J., Yi J.Y., Noh D.Y., Shin I. CD24 enhances DNA

damage-induced apoptosis by modulating NF-κB signaling in CD44-expressing breast cancer cells. *Carcinogenesis*, 32: 1474-1483, 2011. doi: 10.1093/carcin/bgr173.

50) Hauser-Kawaguchi A., Luyt L.G., Turley E. Design of peptide mimetics to block pro-inflammatory functions of HA fragments. *Matrix Biol*, 78–79: 346–356, 2019. doi: 10.1016/j.matbio.2018.01.021.

51) Xu Y., Kiningham K.K., Devalaraja M.N., Yeh C.C., Majima H., Kasarskis E.J., St Clair D.K. An intronic NF-kappaB element is essential for induction of the human manganese superoxide dismutase gene by tumor necrosis factor-alpha and interleukin-1beta. *DNA Cell Biol*, 18: 709–722, 1999. doi: 10.1089/104454999314999.

52) Thorne R.F., Legg J.W., Isacke C.M. The role of the CD44 transmembrane and cytoplasmic domains in co-ordinating adhesive and signalling events. *J. Cell Sci*, 117: 373–380, 2004. doi: 10.1242/jcs.00954.

53) Abdraboh M.E., Gaur R.L., Hollenbach A.D., Sandquist D., Raj M.H., Ouhtit A. Survivin is a novel target of CD44-promoted breast tumor invasion. *Am. J. Pathol*, 179: 555–563, 2011. doi: 10.1016/j.ajpath.2011.04.042.

54) Brinck J., Heldin P. Expression of recombinant hyaluronan synthase (HAS) isoforms in CHO cells reduces cell migration and cell surface CD44. *Exp. Cell Res*, 252: 342–351, 1999. doi: 10.1006/excr.1999.4645.

55) Evanko S.P., Wight T.N. Intracellular localization of hyaluronan in proliferating cells. *J. Histochem. Cytochem*, 47: 1331–1342, 1999. doi: 10.1177/002215549904701013.

56) Evanko S.P., Parks W.T., Weight T.N. Intracellular hyaluronan in arterial smooth muscle cells, association with microtubules, RHAMM, and the mitotic spindle. *J. Histochem. Cytochem*, 52: 1525–1535, 2004. doi: 10.1369/jhc.4A6356.2004.

57) Ren J., Hascall V.C., Wang A. Cyclin, D3 mediates synthesis of a hyaluronan matrix that is adhesive for monocytes in mesangial cells stimulated to divide in hyperglycemic medium. *J. Biol. Chem*, 284: 16621–16632, 2009. doi: 10.1074/jbc.M806430200.

58) Bohaumilitzky L., Huber A.K., Stork E.M., Wengert S., Woelfl F., Boehm H. A Trickster in Disguise: Hyaluronan's Ambivalent Roles in the Matrix. *Front. Oncol*, 7: 242, 2017. doi:

10.3389/fonc.2017.00242.

59) Misra S., Hascall V.C., Markwald R.R., Ghatak S. Interactions between Hyaluronan and Its Receptors (CD44, RHAMM) Regulate the Activities of Inflammation and Cancer. *Front. Immunol*, 6: 201, 2015. doi: 10.3389/fimmu.2015.00201.

60) Lee J.L., Wang M.J., Chen J.Y. Acetylation and activation of STAT3 mediated by nuclear translocation of CD44. *J. Cell Biol*, 185: 949–957, 2009. doi: 10.1083/jcb.200812060.

61) Skandalis S.S., Karalis T., Heldin P. Intracellular hyaluronan: Importance for cellular functions. *Semin. Cancer Biol*, 60: 20–30, 2020. doi: 10.1016/j.semcancer.2019.07.002.

62) Assmann V., Marshall F.J., Fieber C., Hofmann M., Hart I.R. The human hyaluronan receptor RHAMM is expressed as an intracellular protein in breast cancer cells. *J. Cell Sci*, 111: 1685–1694, 1998. doi: 10.1242/jcs.111.12.1685.

63) Pilarski L.M., Masellis-Smith A., Belch A.R., Yang B., Savani R.C., Turley E.A. RHAMM, a receptor for hyaluronan-mediated motility, on normal human lymphocytes, thymocytes and malignant B cells: A mediator in B cell malignancy? *Leuk. Lymphoma*, 14: 363–374, 1994. doi: 10.3109/10428199409049691.

64) Yang B., Yang B.L., Savani R.C., Turley E.A. Identification of a common hyaluronan binding motif in the hyaluronan binding proteins RHAMM, CD44 and link protein. *EMBO J*, 13: 286–296, 1994. doi: 10.1002/j.1460-2075.1994.tb06261.x.

65) Nguyen N., Kumar A., Chacko S., Ouellette R.J., Ghosh A. Human hyaluronic acid synthase-1 promotes malignant transformation via epithelial-to-mesenchymal transition, micronucleation and centrosome abnormalities. *Cell Commun. Signal*, 15: 48, 2017. doi: 10.1186/s12964-017-0204-z.

66) Kuo Y.Z., Fang W.Y., Huang C.C., Tsai S.T., Wang Y.C., Yang C.L., Wu L.W. Hyaluronan synthase 3 mediated oncogenic action through forming inter-regulation loop with tumor necrosis factor alpha in oral cancer. *Oncotarget*, 8: 15563–15583, 2017. doi: 10.18632/oncotarget.14697.

67) Krishnan R., Thayalan D.K., Padmanaban R., Ramadas R., Annasamy R.K., Anandan N. Association of serum and salivary tumor necrosis factor-alpha with histological grading in oral

cancer and its role in differentiating premalignant and malignant oral disease. *Asian Pac. J. Cancer Prev*, 15: 7141–7148, 2014. doi: 10.7314/APJCP.2014.15.17.7141.

Abstract

4-メチルウンベリフェロンによる放射線抵抗性癌細胞の放射線増感効果の検討

長谷川　和輝

弘前大学大学院保健学研究科　放射線技術科学領域

放射線抵抗性細胞は、放射線治療後の腫瘍の再発や遠隔転移を引き起こし、予後不良の一因と考えられている。これまでの研究で、ヒアルロン酸 (HA)合成阻害剤として知られている 4-メチルウンベリフェロン (4-MU)は、様々な癌細胞で HA 合成酵素 (HAS)の発現抑制を介して抗腫瘍効果や抗転移効果を発揮することが示されている。さらに、ヒト線維肉腫細胞 HT1080 に対して 4-MU 投与と X 線照射を併用することにより、放射線増感効果が増強されることが明らかとなっている。しかし、放射線抵抗性細胞に対する放射線増感戦略は確立されておらず、4-MU が放射線抵抗性細胞に対して放射線増感効果を発揮するかどうかは不明である。そこで本研究では、長期的な分割照射により放射線抵抗性を獲得した口腔扁平上皮癌細胞株を使用し、4-MU の放射線増感剤としての効果を検討した。

本研究結果では、4-MU 投与によって放射線抵抗性細胞の細胞生存率や細胞遊走が抑制され、抗腫瘍効果が増強されることが示されたが、放射線増感効果は誘導されなかった。また、癌幹細胞様表現型が抑制され、細胞内酸化ストレスが増強されることが示唆された。さらに、4-MU の作用機序として HA 阻害に着目し、HA 分解酵素による細胞外 HA 除去あるいは siRNA による HAS ノックダウンを実施した。本研究で使用した放射線抵抗性細胞株では、親細胞株と比較して HAS3 mRNA 発現が有意に高いことから、HAS3 をノックダウン標的とした。細胞外 HA の除去は放射線増感効果を誘導しなかったが、HAS3 ノックダウンによって放射線増感効果の増強が観察された。また、HA 受容体である CD44 発現や癌幹細胞様表現型の抑制、酸化ストレスの増強も示された。

HA/CD44 の相互作用は細胞生存を促進するシグナル伝達に重要であるが、細胞外 HA の除去のみでは放射線増感効果が誘導されず、HAS3 抑制によって誘導されたことを考慮すると、HAS3 を介した HA 合成を阻害することによって、CD44 の経路を抑制させることが放射線増感効果につながることが示唆された。一方で、もう一つの主要な受容体である RHAMM は、細胞内外で HA と相互作用することが報告されている。さらに、TNF-α は HAS3 と相互調節ループを形成することで腫瘍形成を促進する。したがって、HAS3 が合成する細胞内ヒアルロン酸の相互作用あるいは HAS3 の直接的な作用が放射線抵抗性に寄与している可能性が示唆された。本研究により、HAS3 を標的とした、放射線抵抗性細胞に対する新たな放射線増感戦略の可能性が示唆された。